Regularized lattice Boltzmann model for a class of convection-diffusion equations

Lei Wang,[1] Baochang Shi,[1,2,*] and Zhenhua Chai[1,2]
[1]*School of Mathematics and Statistics, Huazhong University of Science and Technology, Wuhan 430074, China*
[2]*State Key Laboratory of Coal Combustion, Huazhong University of Science and Technology, Wuhan 430074, China*
(Received 6 July 2015; published 30 October 2015)

In this paper, a regularized lattice Boltzmann model for a class of nonlinear convection-diffusion equations with variable coefficients is proposed. The main idea of the present model is to introduce a set of precollision distribution functions that are defined only in terms of macroscopic moments. The Chapman-Enskog analysis shows that the nonlinear convection-diffusion equations can be recovered correctly. Numerical tests, including Fokker-Planck equations, Buckley-Leverett equation with discontinuous initial function, nonlinear convection-diffusion equation with anisotropic diffusion, are carried out to validate the present model, and the results show that the present model is more accurate than some available lattice Boltzmann models. It is also demonstrated that the present model is more stable than the traditional single-relaxation-time model for the nonlinear convection-diffusion equations.

DOI: 10.1103/PhysRevE.92.043311 PACS number(s): 02.70.−c, 02.60.Cb, 44.05.+e

I. INTRODUCTION

The lattice Boltzmann method (LBM), as a kinetic-based numerical method, has gained a great success in the study of complex hydrodynamic problems across a broad range of scales [1–3]. Compared with the traditional computational fluid dynamics method based on the macroscopic continuum equations, it has some distinct advantages, such as easy implementation of boundary conditions and parallelism. Simultaneously, the LBM has also been shown to have potential in solving some partial differential equations [4–7], including the widely encountered nonlinear convection-diffusion equations (NCDEs), which have been used to describe the heat and mass transport caused by the diffusion and advection processes.

Actually, there exist many lattice Boltzmann (LB) models for the NCDEs [8–17,30]. van der Sman *et al.* [8] developed an LB model for the NCDE with irregular lattices. In their work, some traditional methods, including finite-difference and finite-element methods, were compared with the LBM, and the results show that the LBM has a comparable performance with these traditional methods. Shi *et al.* [9] proposed a scheme for source term in the LBM for NCDEs, in which a differential operator of the source term is added to the evolution equation. Shi and Guo [10] also presented a LB model for the NCDE. Unlike some previous models, an auxiliary moment is introduced in this model such that the NCDE with a source term can be recovered, and also, this model can be used to solve the real and complex-valued nonlinear evolutionary equations and NCDEs with anisotropic diffusion [11]. For the NCDEs with anisotropic diffusion, some LB models have also been proposed [12–15]. Ginzburg [12] presented the equilibrium-type and link-type models to handle the NCDEs with anisotropic diffusion, and recently, the author also summarized some alternative ways to study anisotropic diffusion problems with a focus on the numerical diffusion [13].

Although many LB models have been proposed for the NCDEs, there are still two limits among these available models. First, as shown by the Chapman-Enskog analysis, there are some additional terms in the corresponding macroscopic equations when the convection term is a function of space or time, which may also influence the accuracy of the LBM [16,17]. Second, the most widely used model for NCDEs is the single relaxation time (SRT) or Bhatnagar-Gross-Krook (BGK) model. As we know, the SRT model is numerically most efficient, but suffers from inaccuracy and instability problems [18,19]. To overcome these two defects, some improved models have also been proposed. Chopard *et al.* [16] constructed an LB model for the CDE, where a time-derivative or space-derivative term is added in the evolution equation, and found that the model with the space-derivative term is more accurate. This method has also been extended to study the multiphase flows [20] and thermal flows [21]. On the other hand, to improve the numerical stability of the SRT model, some improvements have also been made in the available works [12,14,22–24], and most of them are based on the the two-relaxation-time (TRT) or multirelaxation-time (MRT) models. The TRT and MRT models are superior over the SRT model for a number of problems, however, as pointed out in Refs. [12,25], the optimal relaxation time of these two models cannot obey universal criteria. Recently, Latt and Chopard proposed a regularized version of the SRT LBM (denoted as RLB model) that offers an improvement in accuracy and stability without introducing any substantial complication with respect to the original SRT model [26]. The main idea of the RLB model is to introduce a set of precollision distribution functions that are defined only in terms of the macroscopic moments, and all the higher-order nonequilibrium information is discarded [27,28]. Recently, the regularized lattice Boltzmann method (RLBM) is also used to investigate the classical lid-driven cavity and Womersley flows [28,29], and the numerical results show that compared to the traditional SRT model, the RLB model is more stable and more accurate.

In this work, we will extend the regularized procedure described in Ref. [26] from fluid dynamics to NCDEs, and present a simple and efficient RLB model for the NCDE with variable coefficients. The Chapman-Enskog analysis shows that the NCDE can be recovered exactly from the present model, and more importantly, the regularized procedure

*Corresponding author: shibc@hust.edu.cn

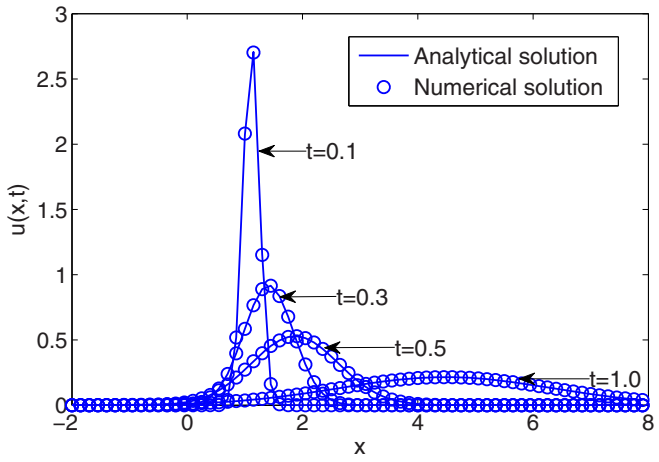

FIG. 1. (Color online) Numerical and analytical solutions of Example 3.1 at different times.

described in this paper can be easily extended to some existing LB models. The rest of the paper is organized as follows. In Sec. II, an RLB model for the NCDE with variable coefficients is developed, and some of its special cases are also discussed. We then performed some tests to validate the present model in Sec. III, and finally, some conclusions are given in Sec. IV.

II. REGULARIZED LATTICE BOLTZMANN MODEL FOR NCDE

In this section, we will present a RLB model for n-dimensional (nD) NCDE with variable coefficients, which can be written as

$$\partial_t\phi + \nabla\cdot\mathbf{B}(\mathbf{x},\phi,t) = \nabla\cdot[\alpha(\mathbf{x},t)\nabla\cdot\mathbf{D}(\mathbf{x},\phi,t)] + F(\mathbf{x},\phi,t), \tag{1}$$

where ϕ is a scalar function of position $\mathbf{x}$ and time t, ∇ is the gradient operator with respect to the position $\mathbf{x}$ in n dimensions. $\mathbf{B}(\mathbf{x},\phi,t)$ and $\mathbf{D}(\mathbf{x},\phi,t)$ are the known convection and diffusion terms, and usually they are related to position $\mathbf{x}$, ϕ, and time t, $\alpha(\mathbf{x},t)$ and $F(\mathbf{x},\phi,t)$ are the diffusion coefficient and source term, respectively.

The evolution equation of the RLB model for the NCDE reads

$$\begin{aligned} f_i(\mathbf{x}+\mathbf{c}_i\Delta t,t+\Delta t) =& f_i^{eq}(\mathbf{x},t) + \left(1-\frac{1}{\tau}\right)\frac{\omega_i\mathbf{c}_i\cdot\mathbf{\Pi}^{(\mathrm{neq})}(x,t)}{c_s^2} \\ &+ \Delta t G_i(\mathbf{x},\phi,t) + \Delta t F_i(\mathbf{x},\phi,t) \\ &+ \frac{\Delta t^2}{2}\partial_t F_i(\mathbf{x},\phi,t),\ i=0,\ldots,q-1, \end{aligned} \tag{2}$$

where $\{\mathbf{c}_i,\ i=0,\ldots,q-1\}$ is the set of discrete velocity, Δt is the time step, τ and ω_i are the dimensionless relaxation time and weight coefficient, respectively.

$$\begin{aligned} \mathbf{\Pi}^{(\mathrm{neq})}(\mathbf{x},t) =& \mathbf{\Pi}(\mathbf{x},t) - \mathbf{\Pi}^{(0)}(\mathbf{x},t) \\ =& \sum_{j=0}^{q-1}\mathbf{c}_j f_j(\mathbf{x},t) - \sum_{j=0}^{q-1}\mathbf{c}_j f_j^{eq}(\mathbf{x},t) \end{aligned}$$

with $f_i(\mathbf{x},t)$ and $f_i^{eq}(\mathbf{x},t)$ representing the local particle distribution function and equilibrium distribution function at position $\mathbf{x}$ and time t. $G_i(\mathbf{x},\phi,t)$ is the correction term to eliminate the additional term [i.e., $(\tau-0.5)\Delta t\nabla\cdot\partial_t B(\mathbf{x},\phi,t)$; see the details in the following Chapman-Enskog analysis] in the corresponding macroscopic equation, and $F_i(\mathbf{x},\phi,t)$ is the distribution function of the source term.

The key point of using Eq. (2) to solve Eq. (1) is to construct proper $f_i^{eq}(\mathbf{x},t)$, $G_i(\mathbf{x},\phi,t)$, and $F_i(\mathbf{x},\phi,t)$ which must satisfy some constraints. Inspired by our previous works [10,11], the equilibrium distribution $f_i^{eq}(x,t)$ and source term $F_i(\mathbf{x},\phi,t)$ are given as

$$f_i^{eq}(\mathbf{x},t) = \omega_i\left[\phi + \frac{\mathbf{c}_i\cdot\mathbf{B}(\mathbf{x},\phi,t)}{c_s^2} + \frac{\left(\mathbf{C}(\mathbf{x},\phi,t) - c_s^2\phi\mathbf{I}\right):\mathbf{Q}_i}{2c_s^4}\right], \tag{3}$$

$$F_i(\mathbf{x},\phi,t) = \omega_i F(\mathbf{x},\phi,t), \tag{4}$$

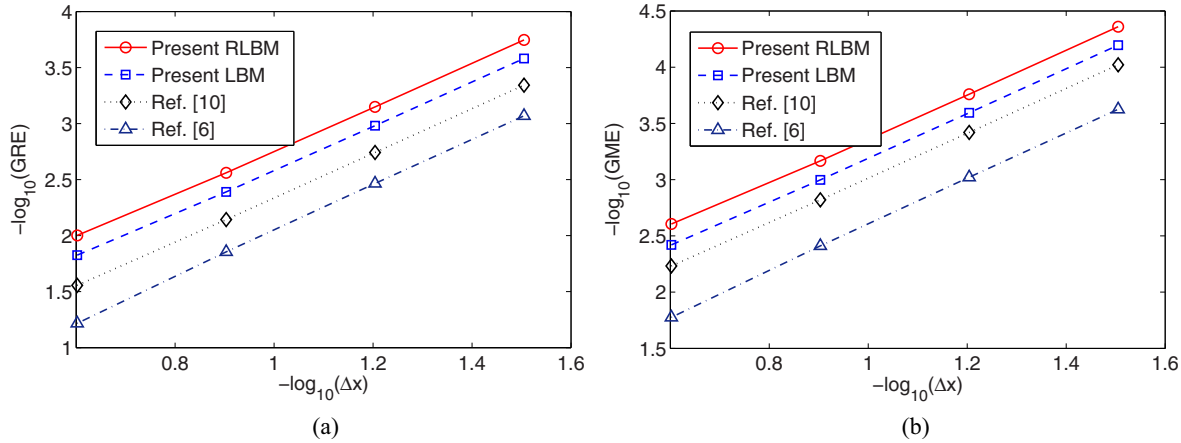

(a) (b)

FIG. 2. (Color online) The errors of different models with different lattice steps for Example 3.1: (a) GREs; (b) GMEs.

TABLE I. Comparison of the GREs and the GMEs at different times for Example 3.1.

t	Error	Present RLBM	Present LBM	Ref. [10]	Ref. [6]
0.50	GRE	4.2282×10^{-4}	5.8181×10^{-4}	5.4382×10^{-4}	7.0312×10^{-4}
	GME	2.3612×10^{-4}	3.2304×10^{-4}	3.1140×10^{-4}	4.1040×10^{-4}
0.75	GRE	2.0061×10^{-4}	2.8410×10^{-4}	3.3324×10^{-4}	5.6469×10^{-4}
	GME	7.0850×10^{-5}	9.9146×10^{-5}	1.0792×10^{-4}	1.8812×10^{-4}
1.00	GRE	1.1475×10^{-4}	1.6812×10^{-4}	2.9057×10^{-4}	5.4461×10^{-4}
	GME	2.7987×10^{-5}	4.0799×10^{-5}	6.0996×10^{-5}	1.5158×10^{-4}
1.25	GRE	9.2022×10^{-5}	1.3701×10^{-4}	4.1127×10^{-4}	6.7231×10^{-4}
	GME	1.2244×10^{-5}	1.8949×10^{-5}	4.9219×10^{-5}	1.4868×10^{-4}
1.50	GRE	1.6516×10^{-4}	2.4023×10^{-4}	1.2395×10^{-3}	2.1250×10^{-3}
	GME	2.6976×10^{-6}	4.0074×10^{-6}	3.2954×10^{-5}	4.9276×10^{-5}

which satisfy the following conditions:

$$\sum_i f_i = \sum_i f_i^{eq} = \phi, \quad \sum_i \mathbf{c}_i f_i^{eq} = \mathbf{B}(\mathbf{x},\phi,t), \quad \sum_i \mathbf{c}_i \mathbf{c}_i f_i^{eq} = \mathbf{C}(\mathbf{x},\phi,t), \tag{5}$$

$$\sum_i F_i = F(\mathbf{x},\phi,t), \quad \sum_i \mathbf{c}_i F_i = 0, \tag{6}$$

where $\mathbf{I}$ is the unit tensor, $\mathbf{Q}_i$ is a tensor, and is defined $\mathbf{Q}_i = \mathbf{c}_i\mathbf{c}_i - c_s^2\mathbf{I}$, c_s is related to the particle velocity c ($c = \Delta x/\Delta t$, Δx is the lattice spacing) and weight coefficient ω_i through the relation $\sum_i \omega_i \mathbf{c}_i\mathbf{c}_i = c_s^2\mathbf{I}$. $\mathbf{C}(\mathbf{x},\phi,t) = c_s^2\beta\mathbf{D}(\mathbf{x},\phi,t)$, β is a parameter, and can be used to adjust the dimensionless relaxation time [30]. The correction term $G_i(\mathbf{x},\phi,t)$ is defined as

$$G_i(\mathbf{x},\phi,t) = \left(1 - \frac{1}{2\tau}\right)\frac{\omega_i \mathbf{c}_i \cdot \partial_t \mathbf{B}}{c_s^2}, \tag{7}$$

which satisfies $\sum_i G_i = 0$ and $\sum_i \mathbf{c}_i G_i = (1 - \frac{1}{2\tau})\partial_t \mathbf{B}$.

In this work, our model is developed based on the $DnQq$ lattice (q is the number of discrete velocity directions in n-dimensional space), where the discrete velocity $\mathbf{c}_i$ and weight ω_i satisfy some isotropic constraints,

$$\sum_{i=0}^{q-1} \omega_i = 1, \quad \sum_{i=0}^{q-1} \mathbf{c}_i \omega_i = \mathbf{0}, \quad \sum_{i=0}^{q-1} \mathbf{c}_i\mathbf{c}_i\omega_i = c_s^2\mathbf{I}, \quad \sum_{i=0}^{q-1} \mathbf{c}_i\mathbf{c}_i\mathbf{c}_i\omega_i = \mathbf{0}, \tag{8}$$

For the $D1Q3$ lattice model, $\{\mathbf{c}_0, \mathbf{c}_1, \mathbf{c}_2\} = \{0, c, -c\}$, $\omega_0 = 2/3$, $\omega_1 = \omega_2 = 1/6$; while for the $D2Q9$ lattice model, $\{\mathbf{c}_j,\ j = 0, \cdots, 8\} = \{(0,0), (\pm c,0), (0, \pm c), (\pm c, \pm c)\}$, $\omega_0 = 4/9$, $\omega_{1\text{–}4} = 1/9$, $\omega_{5\text{–}8} = 1/36$. We note that $c_s^2 = c^2/3$ is satisfied in both models. Besides, from Eq. (8), we can obtain

$$\sum_{i=0}^{q-1} \omega_i \mathbf{Q}_i = \mathbf{0}, \quad \sum_{i=0}^{q-1} \omega_i \mathbf{c}_i \mathbf{Q}_i = \mathbf{0}. \tag{9}$$

In what follows, we will perform a detailed Chapman-Enskog analysis to derive Eq. (1). To this end, we first expand the distribution function f_i, the derivatives of the space and time as

$$f_i = f_i^{(0)} + \varepsilon f_i^{(1)} + \varepsilon^2 f_i^{(2)} + \cdots,$$
$$G = \varepsilon G^{(1)} + \varepsilon^2 G^{(2)}, \tag{10}$$
$$F = \varepsilon F^{(1)}, \quad \partial_t = \varepsilon\partial_{t_1} + \varepsilon^2\partial_{t_2}, \quad \nabla = \varepsilon\nabla_1,$$

where ε is a small parameter. Taking the Taylor series expansion to Eq. (2) at time t and space $\mathbf{x}$, we have

$$f_i + \Delta t D_i f_i + \frac{\Delta t^2}{2} D_i^2 f_i + \cdots = f_i^{(eq)} + \left(1 - \frac{1}{\tau}\right)\frac{\omega_i \mathbf{c}_i}{c_s^2} \cdot \mathbf{\Pi}^{(\mathrm{neq})} + \Delta t G_i + \Delta t F_i + \frac{\Delta t^2}{2}\partial_t F_i, \tag{11}$$

where $D_i = \varepsilon D_{1i} + \varepsilon^2\partial_{t_2}$ with $D_{1i} = \partial_{t_1} + \mathbf{c}_i \cdot \nabla_1$. Substituting Eq. (10) into Eq. (11) yields the following equation:

$$f_i^{(0)} + \varepsilon f_i^{(1)} + \varepsilon^2 f_i^{(2)} + \Delta t\left(\varepsilon D_{1i} + \varepsilon^2\partial_{t_2}\right)\left(f_i^{(0)} + \varepsilon f_i^{(1)} + \varepsilon^2 f_i^{(2)}\right) + \frac{\Delta t^2}{2}\left(\varepsilon D_{1i} + \varepsilon^2\partial_{t_2}\right)^2\left(f_i^{(0)} + \varepsilon f_i^{(1)} + \varepsilon^2 f_i^{(2)}\right)$$
$$= f_i^{(eq)} + \left(1 - \frac{1}{\tau}\right)\frac{\omega_i \mathbf{c}_i}{c_s^2} \cdot \sum_{j=0}^{q-1} \mathbf{c}_j\left(f_j^{(0)} + \varepsilon f_j^{(1)} + \varepsilon^2 f_j^{(2)} - f_j^{eq}\right) + \Delta t\varepsilon G_i^{(1)} + \Delta t\varepsilon^2 G_i^{(2)} + \Delta t\varepsilon F_i^{(1)} + \frac{\Delta t^2}{2}\left(\varepsilon^2\partial_{t_1} + \varepsilon^3\partial_{t_2}\right)F_i^{(1)}. \tag{12}$$

TABLE II. Comparison of the GREs among different models for Example 3.1 ($t = 1.0$, $c = 150$).

N	Present RLBM	Present LBM	Ref. [10]	Ref. [6]
160	4.7964×10^{-4}	2.5912×10^{-4}	5.2102×10^{-4}	6.4933×10^{-4}
320	1.8624×10^{-4}	3.0951×10^{-4}	5.2020×10^{-4}	9.8464×10^{-4}
640	1.2031×10^{-4}	3.7537×10^{-4}	5.4580×10^{-4}	1.0690×10^{-3}
1280	1.5392×10^{-4}	3.9272×10^{-4}	5.5324×10^{-4}	1.0882×10^{-3}

Based on Eq. (12), we can derive the equations at different orders of ε,

$$\mathrm{O}(\varepsilon^0)\ f_i^{(0)} = f_i^{(eq)} + \left(1 - \frac{1}{\tau}\right)\frac{\omega_i}{c_s^2}\mathbf{c}_i \cdot \sum_{j=0}^{q-1}\mathbf{c}_j\left(f_j^{(0)} - f_j^{(eq)}\right), \tag{13}$$

$$\mathrm{O}(\varepsilon^1)\ f_i^{(1)} + \Delta t D_{1i} f_i^{(0)} = \left(1 - \frac{1}{\tau}\right)\frac{\omega_i}{c_s^2}\mathbf{c}_i \cdot \sum_{j=0}^{q-1}\mathbf{c}_j f_j^{(1)} + \Delta t G_i^{(1)} + \Delta t F_i^{(1)}, \tag{14}$$

$$\mathrm{O}(\varepsilon^2)\ f_i^{(2)} + \Delta t\left(\partial_{t_2} f_i^{(0)} + D_{1i} f_i^{(1)}\right) + \frac{\Delta t^2}{2} D_{1i}^2 f_i^{(0)} = \left(1 - \frac{1}{\tau}\right)\frac{\omega_i}{c_s^2}\mathbf{c}_i \cdot \sum_{j=0}^{q-1}\mathbf{c}_j f_j^{(2)} + \Delta t G_i^{(2)} + \frac{\Delta t^2}{2}\partial_{t_1} F_i^{(1)}. \tag{15}$$

Multiplying Eq. (13) by $\mathbf{c}_i$ and summing it over i, one can obtain

$$\sum_{i=0}^{q-1}\mathbf{c}_i f_i^{(0)} = \sum_{i=0}^{q-1}\mathbf{c}_i f_i^{(eq)} + \left(1 - \frac{1}{\tau}\right)\frac{1}{c_s^2}\sum_{i=0}^{q-1}\omega_i \mathbf{c}_i \mathbf{c}_i \cdot \sum_{j=0}^{q-1}\mathbf{c}_j\left(f_j^{(0)} - f_j^{(eq)}\right). \tag{16}$$

With the aid of Eq. (8), we can get

$$\sum_{i=0}^{q-1}\mathbf{c}_i f_i^{(0)} = \sum_{i=0}^{q-1}\mathbf{c}_i f_i^{(eq)}. \tag{17}$$

Substituting Eq. (17) into Eq. (13), we can derive the following equation:

$$f_i^{(0)} = f_i^{(eq)}, \tag{18}$$

then from Eqs. (5), (10), and (18), the mass conservation condition can be obtained,

$$\sum_{i=0}^{q-1} f_i^{(k)} = 0\ (k \geqslant 1). \tag{19}$$

Applying Eq. (14) to the left side of the Eq. (15), we have

$$f_i^{(2)} + \Delta t\partial_{t_2} f_i^{(0)} + \frac{\Delta t}{2} D_{1i} f_i^{(1)} + \frac{\Delta t}{2} D_{1i}\left[\left(1 - \frac{1}{\tau}\right)\frac{\omega_i \mathbf{c}_i}{c_s^2} \cdot \sum_{j=0}^{q-1}\mathbf{c}_j f_j^{(1)}\right] + \frac{\Delta t^2}{2} D_{1i}\left(G_i^{(1)} + F_i^{(1)}\right)$$

$$= \left(1 - \frac{1}{\tau}\right)\frac{\omega_i}{c_s^2}\mathbf{c}_i \cdot \sum_{j=0}^{q-1}\mathbf{c}_j f_j^{(2)} + \Delta t G_i^{(2)} + \frac{\Delta t^2}{2}\partial_{t_1} F_i^{(1)}. \tag{20}$$

Summing Eqs. (14) and (20) over i and using Eqs. (5), (6), (8), and (18), we can obtain

$$\partial_{t_1}\phi + \nabla_1 \cdot \mathbf{B}(\mathbf{x}, \phi, t) = F^{(1)}, \tag{21}$$

$$\partial_{t_2}\phi + \nabla_1 \cdot \left[\left(1 - \frac{1}{2\tau}\right)\sum_{i=0}^{q-1}\mathbf{c}_i f_i^{(1)}\right] + \frac{\Delta t}{2}\nabla_1 \cdot \left[\left(1 - \frac{1}{2\tau}\right)\partial_{t_1}\mathbf{B}\right] = 0. \tag{22}$$

Based on Eq. (14), we have

$$\sum_{i=0}^{q-1}\mathbf{c}_i f_i^{(1)} = -\Delta t\left(\partial_{t_1}\sum_{i=0}^{q-1}\mathbf{c}_i f_i^{(0)} + \nabla_1 \cdot \sum_{i=0}^{q-1}\mathbf{c}_i \mathbf{c}_i f_i^{(0)}\right) + \left(1 - \frac{1}{\tau}\right)\frac{1}{c_s^2}\sum_{i=0}^{q-1}\omega_i \mathbf{c}_i \mathbf{c}_i \cdot \sum_{j=0}^{q-1}\mathbf{c}_j f_j^{(1)} + \Delta t\sum_{i=0}^{q-1}\mathbf{c}_i G_i^{(1)}, \tag{23}$$

TABLE III. GREs of Example 3.1 with different β and c ($\Delta x = 0.1$, $t = 1.0$).

β	c	Present RLBM	Present LBM	Ref. [10]	Ref. [6]
0.75	60	1.1220×10^{-3}	5.2800×10^{-3}	6.4712×10^{-3}	1.0652×10^{-2}
	120	2.7866×10^{-4}	1.2679×10^{-3}	1.5834×10^{-3}	2.5724×10^{-3}
1.00	60	8.8911×10^{-4}	2.4308×10^{-3}	3.4371×10^{-3}	6.8515×10^{-3}
	120	1.9327×10^{-4}	5.6337×10^{-4}	8.4298×10^{-4}	1.6447×10^{-3}
1.25	60	7.4445×10^{-4}	1.3147×10^{-3}	2.2439×10^{-3}	5.0155×10^{-3}
	120	1.4320×10^{-4}	2.8415×10^{-4}	5.5334×10^{-4}	1.1951×10^{-3}

then substituting Eq. (8) into Eq. (23), one can obtain

$$\begin{aligned}\sum_{i=0}^{q-1}\mathbf{c}_i f_i^{(1)} =& -\tau\Delta t\left(\partial_{t_1}\sum_{i=0}^{q-1}\mathbf{c}_i f_i^{(0)} + \nabla_1\cdot\sum_{i=0}^{q-1}\mathbf{c}_i\mathbf{c}_i f_i^{(0)}\right) + \tau\Delta t\sum_{i=0}^{q-1}\mathbf{c}_i G_i^{(1)}\\ =& -\tau\Delta t\left(\partial_{t_1}\mathbf{B} + c_s^2\beta\nabla_1\cdot\mathbf{D}\right) + \tau\Delta t\left[\left(1-\frac{1}{2\tau}\right)\partial_{t_1}\mathbf{B}\right]\\ =& -\tau\Delta t c_s^2\beta\nabla_1\cdot\mathbf{D} - \frac{\Delta t}{2}\partial_{t_1}\mathbf{B}.\end{aligned} \tag{24}$$

With the help of the above equation, Eq. (22) can be rewritten as

$$\partial_{t_2}\phi - \nabla_1\cdot\left[c_s^2\left(\tau-\frac{1}{2}\right)\Delta t\beta\nabla_1\cdot\mathbf{D}(\mathbf{x},\phi,t)\right] = 0. \tag{25}$$

Taking Eq. (21)$\times\varepsilon+$ Eq. (25)$\times\varepsilon^2$, we can obtain the recovered equation,

$$\partial_t\phi + \nabla\cdot\mathbf{B}(\mathbf{x},\phi,t) = \nabla\cdot[\alpha(\mathbf{x},\phi,t)\nabla\cdot\mathbf{D}(\mathbf{x},\phi,t)] + F(\mathbf{x},\phi,t), \tag{26}$$

with

$$\alpha(\mathbf{x},\phi,t) = c_s^2\left(\tau-\frac{1}{2}\right)\Delta t\beta. \tag{27}$$

Now, some remarks on the present model are listed as follows.

Remark 1. From the above Chapman-Enskog analysis, it is clear that $f_i^{(0)}(\mathbf{x},t) = f_i^{(eq)}(\mathbf{x},t)$ at the zero order in ε is still satisfied, and the present model can be viewed as a general solver for the NCDEs with variable coefficients.

Remark 2. The key of the RLB model is that $f_i^{(\mathrm{neq})}$ can be approximated by

$$f_i^{(\mathrm{neq})} \approx \frac{\omega_i\mathbf{c}_i\cdot\mathbf{\Pi}^{(\mathrm{neq})}}{c_s^2}, \tag{28}$$

which can be derived from the Chapman-Enskog analysis. Keeping this in mind, Eq. (2) can also be rewritten as

$$\begin{aligned}f_i(\mathbf{x}+\mathbf{c}_i\Delta t,t+\Delta t) = f_i^{(eq)}(\mathbf{x},t) + \left(1-\frac{1}{\tau}\right)f_i^{(\mathrm{neq})}(\mathbf{x},t) + \Delta t G_i(\mathbf{x},\phi,t) + \Delta t F_i(\mathbf{x},\phi,t) + \frac{\Delta t^2}{2}\partial_t F_i(\mathbf{x},\phi,t),\\ i = 0,\ldots,q-1.\end{aligned} \tag{29}$$

As described in Eq. (29), the evolution of the particle distribution function f_i depends only on the scalar variable ϕ and the nonequilibrium distribution function. And $f_i^{(\mathrm{neq})} = f_i - f_i^{(eq)}$, which can be used to derive the corresponding SRT model for Eq. (1),

$$f_i(\mathbf{x}+\mathbf{c}_i\Delta t,t+\Delta t) - f_i(\mathbf{x},t) = -\frac{1}{\tau}(f_i(\mathbf{x},t) - f_i^{(eq)}(\mathbf{x},t)) + \Delta t G_i(\mathbf{x},\phi,t) + \Delta t F_i(\mathbf{x},\phi,t) + \frac{\Delta t^2}{2}\partial_t F_i(\mathbf{x},\phi,t), \quad i = 0,\ldots,q-1. \tag{30}$$

Actually, compared to the standard LBM, a modified nonequilibrium distribution function has been used to replace the traditional nonequilibrium part such that the stability and accuracy of the LBM can be improved. In addition, the regularized procedure described above can be easily extended to some other LB models for NCDEs [9–11,17,30].

Remark 3. It should be noted that when $\mathbf{B}(\mathbf{x},\phi,t) = 0$, Eq. (1) becomes the diffusion equation with a source term, then the equilibrium distribution function f_i^{eq}, correction term G_i, and distribution function of the source term F_i can be

simplified,

$$f_i^{eq}(x,t) = \omega_i\left[\phi + \frac{\left(\mathbf{C}(\mathbf{x},\phi,t) - c_s^2\phi I\right) : \mathbf{Q}_i}{2c_s^4}\right], \tag{31}$$

$$G_i = 0, \quad F_i = \omega_i F, \tag{32}$$

which are the same as those in Ref. [10].

Remark 4. When the diffusion term $\mathbf{D}(\phi)$ is a linear function of ϕ [e.g., $\mathbf{D}(\phi) = \phi\mathbf{I}$], the equilibrium distribution function $f_i^{(eq)}$ can be simply taken as

$$f_i^{(eq)}(\mathbf{x},t) = \omega_i\left[\phi + \frac{\mathbf{c}_i \cdot \mathbf{B}(\mathbf{x},\phi,t)}{c_s^2}\right]. \tag{33}$$

For this special case, the $DnQ2n$ or $DnQ(2n+1)$ model can be used.

Remark 5. It can be found from the above analysis that the present RLBM is only described by two quantities ϕ and $\mathbf{\Pi}$, which can be computed from the distribution functions f_i and $f_i^{(eq)}$. Actually, based on Eqs. (2) and (5), we can obtain

$$\phi(\mathbf{x},t+\Delta t) = \sum_{i=0}^{q-1} f_i^{(eq)}(\mathbf{x}-\mathbf{c}_i\Delta t,t) + \frac{(1-1/\tau)}{c_s^2}\sum_{i=0}^{q-1}[\omega_i\mathbf{c}_i\cdot(\mathbf{\Pi}(\mathbf{x}-\mathbf{c}_i\Delta t,t) - \mathbf{\Pi}^{(0)}(\mathbf{x}-\mathbf{c}_i\Delta t,t))]$$
$$+ \Delta t\sum_{i=0}^{q-1}\left[G_i(\mathbf{x}-\mathbf{c}_i\Delta t,\phi,t) + F_i(\mathbf{x}-\mathbf{c}_i\Delta t,\phi,t) + \frac{\Delta t}{2}\partial_t F_i(\mathbf{x}-\mathbf{c}_i\Delta t,\phi,t)\right], \tag{34}$$

$$\mathbf{\Pi}(\mathbf{x},t+\Delta t) = \sum_{i=0}^{q-1}\mathbf{c}_i f_i^{(eq)}(\mathbf{x}-\mathbf{c}_i\Delta t,t) + \frac{(1-1/\tau)}{c_s^2}\sum_{i=0}^{q-1}[\omega_i\mathbf{c}_i\mathbf{c}_i\cdot(\mathbf{\Pi}(\mathbf{x}-\mathbf{c}_i\Delta t,t) - \mathbf{\Pi}^{(0)}(\mathbf{x}-\mathbf{c}_i\Delta t,t))]$$
$$+ \Delta t\sum_{i=0}^{q-1}\left[\mathbf{c}_i G_i(\mathbf{x}-\mathbf{c}_i\Delta t,\phi,t) + \mathbf{c}_i F_i(\mathbf{x}-\mathbf{c}_i\Delta t,\phi,t) + \frac{\Delta t}{2}\partial_t\mathbf{c}_i F_i(\mathbf{x}-\mathbf{c}_i\Delta t,\phi,t)\right]. \tag{35}$$

Here we would like to point out that the evolution Eq. (2) in the RLB model can be replaced by Eqs. (34) and (35), where only the macroscopic variables ϕ and $\mathbf{\Pi}$ are used. And simultaneously, the nonequilibrium extrapolation method proposed by Guo *et al.* [31] can be also used to treat boundary conditions, which seems easier to be conducted.

III. NUMERICAL SIMULATION

In this section, we presented several numerical tests to validate the RLB model. The nonequilibrium extrapolation scheme proposed by Guo *et al.* [31] is employed to treat the boundary conditions. Besides, the $D1Q3$ and $D2Q9$ lattice models are used for the tested one-dimensional (1D) and 2D problems, and the backward difference scheme is used to compute $\partial_t F(\mathbf{x},\phi,t)$ and $\partial_t\mathbf{B}(\mathbf{x},\phi,t)$,

$$\frac{\partial F(\mathbf{x},\phi,t)}{\partial t} = \frac{F(\mathbf{x},\phi,t) - F(\mathbf{x},\phi,t-\Delta t)}{\Delta t}, \tag{36}$$

$$\frac{\partial\mathbf{B}(\mathbf{x},\phi,t)}{\partial t} = \frac{\mathbf{B}(\mathbf{x},\phi,t) - \mathbf{B}(\mathbf{x},\phi,t-\Delta t)}{\Delta t}. \tag{37}$$

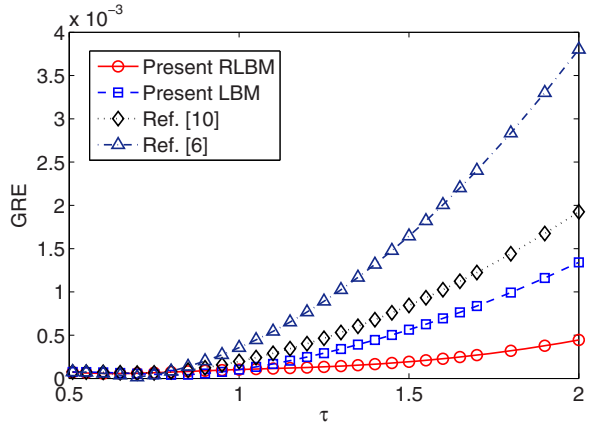

FIG. 3. (Color online) The GREs of different models at different relaxation times (Example 3.1).

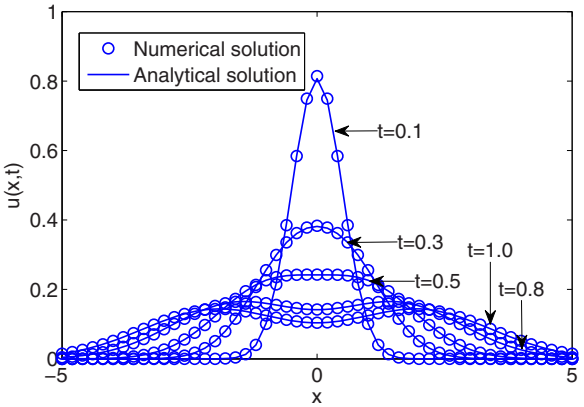

FIG. 4. (Color online) Numerical and analytical solutions of Example 3.2 at different times.

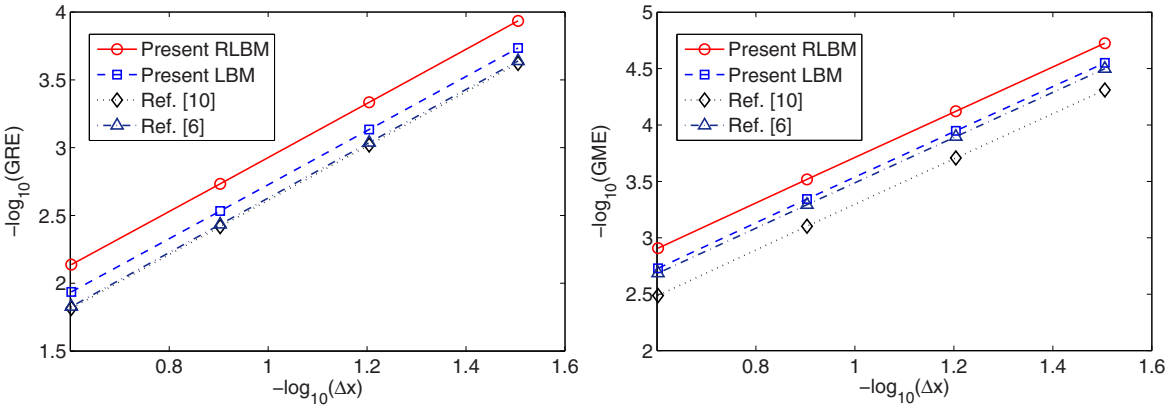

FIG. 5. (Color online) The errors of different models with different lattice steps for Example 3.2: (a) GREs; (b) GMEs.

Here we note that although the use of the backward difference scheme will bring larger memory consumption, it can produce more accurate results.

In our simulations, the global relative error (GRE) and the global maximum error (GME) are used to test the accuracy of the present model, and can be defined as

$$\mathrm{GRE} = \frac{\sum_j |\phi(\mathbf{x}_j,t) - \phi^*(\mathbf{x}_j,t)|}{\sum_j |\phi^*(\mathbf{x}_j,t)|}, \tag{38}$$

$$\mathrm{GME} = \max_j |\phi(\mathbf{x}_j,t) - \phi^*(\mathbf{x}_j,t)|, \tag{39}$$

where $\phi(\mathbf{x}_j,t)$ and $\phi^*(\mathbf{x}_j,t)$ are the numerical and analytical solutions, respectively. The summation is taken over all grid points.

For simplicity, in the following numerical tests, we denote the RLB model given in Eq. (2) and the SRT model given in Eq. (30) as present RLBM and present LBM, respectively. To further show the capacity of the present models, we also compare the present models with the model proposed by Wu *et al.* [6] and the model presented by Shi *et al.* [10]. Unless otherwise stated, the RLB model is used in our simulations and the distribution function $f_i(\mathbf{x},t)$ is initialized by $f_i^{(eq)}(\mathbf{x},t)$ for all nodes at $t = 0$. Here it should be noted that for the initial condition with the Dirac condition, i.e., $\phi(\mathbf{x},0) = \delta(\mathbf{x} - \mathbf{x}_0)$, where

$$\delta(\mathbf{x} - \mathbf{x}_0) = \begin{cases} \infty, & \mathbf{x} = \mathbf{x}_0, \\ 0, & \mathbf{x} \neq \mathbf{x}_0, \end{cases} \tag{40}$$

$$\int_{-\infty}^{+\infty} \delta(\mathbf{x} - \mathbf{x}_0) = 1, \tag{41}$$

the initial condition of $\phi(\mathbf{x},0)$ is taken as

$$\phi(\mathbf{x}_j,0) = \begin{cases} \frac{1}{\Delta\mathbf{x}}, & |\mathbf{x}_j - \mathbf{x}_0| \leqslant \eta, \\ 0, & \mathbf{x} \neq \mathbf{x}_0, \end{cases} \tag{42}$$

where $\Delta\mathbf{x}$ is the lattice spacing, η is a small constant [6].

Example 3.1. We first performed a test of the present RLB model by the following nonlinear Fokker-Planck equation [6]:

$$\frac{\partial u}{\partial t} + \frac{\partial\{[tx + \langle x(t)\rangle]u\}}{\partial x} = \frac{\partial^2(2tu)}{\partial x^2}, \tag{43}$$

with the initial condition

$$u(x,0) = \delta(x - 1.0).$$

The analytical solution of the problem can be given as [6]

$$u(x,t) = \frac{1}{\sqrt{4\pi\eta(t)\exp(t^2)}} \exp\left\{-\frac{[x - \langle x(t)\rangle]^2}{4\eta(t)\exp(t^2)}\right\}, \tag{44}$$

where $\eta(t) = 1 - \exp(-t^2)$, $\langle x(t)\rangle = \exp(t + \frac{t^2}{2})$.

In our simulations, the computational domain is fixed on $\Omega = [-2,8]$. The initial macroscopic variable $u(x,0)$ is zero except for the point at $x_i = 1$ with $u(1,0) = 40$. We present the results at different times in Fig. 1. As seen from this figure, the numerical results agree well with the corresponding analytical solutions. Besides, we also note that although the solution has an abrupt change at $t = 0.1$, the present RLBM still works well.

TABLE IV. GREs of Example 3.2 with different β and c ($\Delta x = 0.1$, $t = 1.0$).

β	c	Present RLBM	Present LBM	Ref. [10]	Ref. [6]
0.75	50	2.5214×10^{-3}	5.6466×10^{-3}	6.4094×10^{-3}	6.1346×10^{-3}
	75	1.3848×10^{-3}	1.6149×10^{-3}	1.9482×10^{-3}	1.7792×10^{-3}
1.00	50	1.1837×10^{-3}	1.8779×10^{-3}	2.4467×10^{-3}	2.3508×10^{-3}
	75	5.8232×10^{-4}	3.1558×10^{-4}	3.8985×10^{-4}	2.6712×10^{-4}
1.25	50	4.9543×10^{-4}	4.1511×10^{-4}	8.2527×10^{-4}	9.0950×10^{-4}
	75	4.2152×10^{-4}	7.1796×10^{-4}	5.2200×10^{-4}	5.7636×10^{-4}

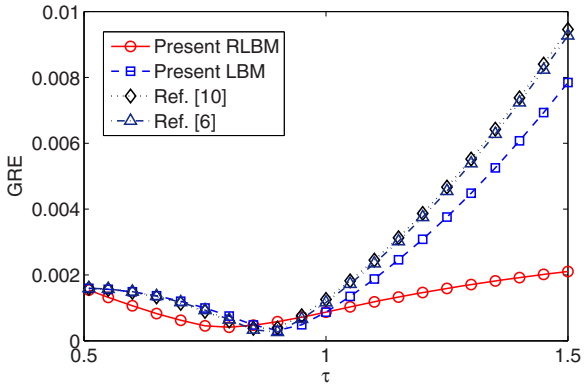

FIG. 6. (Color online) The GREs of different models at different relaxation time (Example 3.2).

To test the convergence rate of the present RLBM, some simulations were carried out at different lattice resolutions ($\Delta x = 1/4$ to $1/32$), and c is correspondingly changed from 20 to 160. As shown in Fig. 2, where the GREs and GMEs at $t = 1.0$ are presented, the slopes of the fitting lines for different results are very close to 2, which indicates that all four models have a second-order convergence rate in space.

In addition, we also conducted a comparison of GREs and GMEs at different times for the case of $\Delta x = 0.025$ and $c = 200$, and presented the results in Table I.

From Table I, one can find that the errors obtained by the present RLBM and LBM are usually less than the other two models, while for the present RLBM and LBM, the RLBM performs better than the LBM, which indicates that the RLB model is more accurate. Besides, we also present the GREs at different resolutions in Table II. As seen from Table II, the numerical results of the present models obtained with 160 grid points are better than or comparable to the numerical results of the other models [6,10] obtained with 320 grid points, which implies the present models are more accurate or more efficient with the same convergent criterion.

In order to study the effects of the parameters β and c, we calculate the GREs under different β and c, and present the results in Table III. From the table it can be found that the GREs decrease with the increase of β and c, and the present RLBM is also more accurate than the other three models.

Finally, we studied the relaxation time effect on the numerical results. For the case of $\Delta x = 0.025$ and $\beta = 1.0$, we compute the GREs under different relaxation times τ, and present the results in Fig. 3 where $t = 1.0$.

As shown in this figure, when the relaxation time τ is smaller than 1, the RLB model is better than or comparable to the other three models, while when the relaxation time is larger than 1, the present RLBM is more accurate than the other three models, and the model in Ref. [6] performs worse since the GREs grow fast with the increase of the relaxation time.

Example 3.2. We also considered another type of the 1D Fokker-Planck equation [32],

$$\frac{\partial u}{\partial t} + \frac{\partial [2\tanh(x)u]}{\partial x} = \frac{\partial u^2}{\partial x^2}, \tag{45}$$

with the analytical solution

$$u(x,t) = \frac{1}{4\pi t}\left\{ \exp\left[-\left(\sqrt{t} + \frac{x}{2\sqrt{t}}\right)^2 \right] + \exp\left[-\left(\sqrt{t} - \frac{x}{2\sqrt{t}}\right)^2 \right] \right\}. \tag{46}$$

The simulations are performed on the domain $[-5, 5]$, and the results are presented in Fig. 4, where $\beta = 0.06$, $\Delta t = 0.0001$, $\Delta x = 0.1$, $u(x,0)$ is zero except for $u(0,0) = 10.0$ at $x = 0.0$. As seen from this figure, the numerical results are in good agreement with the exact solutions. Besides, it can also be found that the numerical solutions transit from a unimodal profile to a bimodal profile at $t = 0.5$, which indicates that the proposed model can also be used to handle unimodality-bimodality transition [32].

To test the convergence rate of the RLB model for this problem, we set $\beta = 1.0$ and performed some simulations under different lattice resolutions ($\Delta x = 1/4 - 1/32$), and c is correspondingly varied from 20 to 160. Based on the GREs and GMEs in Fig. 5, it can be found that the slopes of the fitting

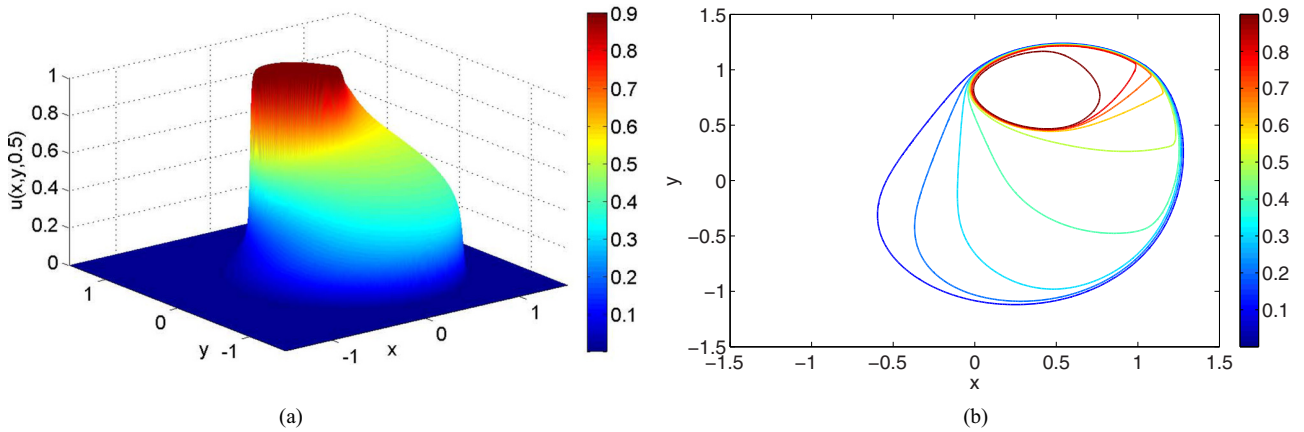

(a) (b)

FIG. 7. (Color online) The distributions (a) and the corresponding contours (b) at $t = 0.5$ for Example 3.3.

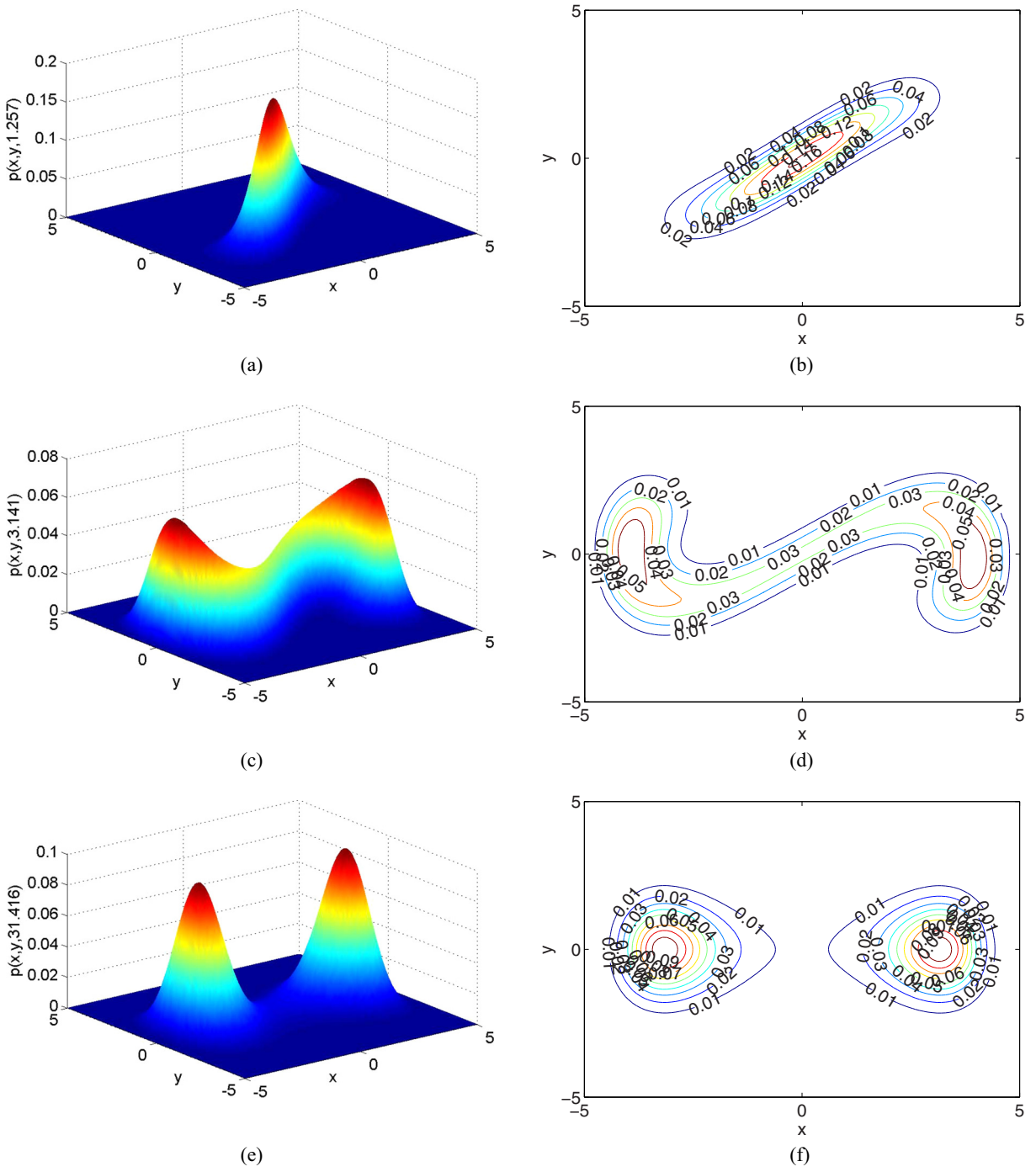

FIG. 8. (Color online) The distributions [(a), (c), (e)] and corresponding contours [(b), (d), (f)] of scale variable $p(x,y,t)$ at different time for Example 3.4.

lines for the results are about 2, indicating that all four models have a second-order accurate convergence rate in space.

Similar to previous discussion, to study the effects of β and c on numerical results, we also computed the GREs under different β and c, and presented them in Table IV. From the table, one can find that when the parameter β is fixed, the GREs decrease obviously with the increase of time step or the increase of the speed c. Besides, it is also found that the present RLBM always performs better than the other three models.

Finally, the same as the discussion in Example 3.1, we also investigated the relaxation time effect. To this end, we first fixed $\Delta x = 0.1$, and $\beta = 1.0$, and then computed the GREs at different relaxation time τ. As shown in Fig. 6 where $t = 1.0$, we can find that there is an optimal relaxation time that can be used to produce the smallest error, and the value is located in the range of [0.75,0.95]. Besides, the difference between GREs of Refs. [6] and [10] is very small, while the present LBM shows a little better performance than those in Refs. [6,10]. And also, the present RLBM seems better

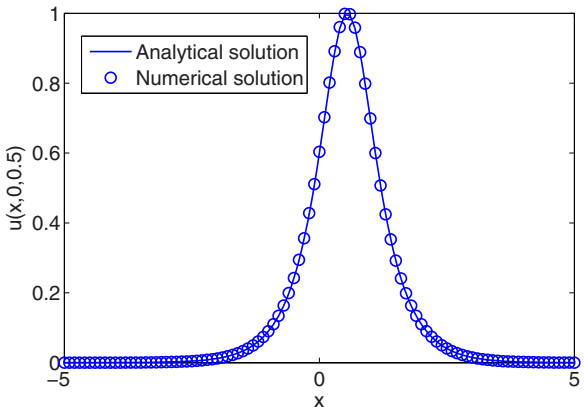

FIG. 9. (Color online) Numerical and analytical solutions of Example 3.5 at $t = 0.5$.

than the other three models, especially when τ approaches 0.5 or exceeds 1.0.

Example 3.3. In this example, we will consider the two-dimensional Buckley-Leverett equation [33]

$$\frac{\partial u}{\partial t} + \frac{\partial f(u)}{\partial x} + \frac{\partial g(u)}{\partial y} = \varepsilon\left(\frac{\partial^2 u}{\partial x^2} + \frac{\partial^2 u}{\partial y^2}\right), \tag{47}$$

with the initial data

$$u(x,y,0) = \begin{cases} 1, & x^2 + y^2 < 0.5, \\ 0, & \text{otherwise}, \end{cases} \tag{48}$$

TABLE VI. GREs of the model [10] incorporated the regularized procedure. (Blanks mean that the model is unstable.)

	$\Delta x = 0.1$		$\Delta x = 0.05$	
t	$c = 10$	$c = 15$	$c = 10$	$c = 15$
0.5	2.1624×10^{-2}	2.4126×10^{-2}	4.6102×10^{-3}	4.9427×10^{-3}
1.0	4.4458×10^{-2}	6.7418×10^{-2}	8.8363×10^{-3}	9.8789×10^{-3}
1.5	6.2927×10^{-2}		1.2281×10^{-2}	1.7452×10^{-2}

where $f(u) = u^2/[u^2 + (1-u)^2], g(u) = f(u)[1-5(1-u)^2]$, $\varepsilon = 0.01$.

We note that the problem is more complicated since there is no analytical solution available. In the following simulations, the computational domain is fixed on $\Omega = [-1.5, 1.5] \times [-1.5, 1.5]$, which is the same as that in Ref. [33]. We presented the numerical solution at $t = 0.5$ in Fig. 7, where $\Delta x = 0.01$ and $c = 100$. As seen from the figure, the results agree well with those reported in Ref. [33].

Example 3.4. Now we consider another 2D Fokker-Planck equation [34],

$$\frac{\partial p(x,y,t)}{\partial t} + \frac{\partial y p(x,y,t)}{\partial x} - \frac{\partial(2\varepsilon y - x + \varsigma x^3)p(x,y,t)}{\partial y} = \frac{\partial^2 (L_{11}x^2 + L_{22})p(x,y,t)}{\partial y^2}, \tag{49}$$

TABLE V. Comparison of GREs at different time for Example 3.5. (Blanks mean that the model is unstable.)

				$D = 0.1$		$D = 0.01$	
Δx	c	Method	t	$d_3 = 0$	$d_3 = 1$	$d_3 = 0$	$d_3 = 1$
0.1	10	Present RLBM	0.5	6.5691×10^{-3}	5.4372×10^{-3}	1.1138×10^{-2}	2.0670×10^{-2}
			1.0	1.7245×10^{-2}	1.5144×10^{-2}	2.8303×10^{-2}	4.5020×10^{-2}
			1.5	2.8083×10^{-2}	2.5276×10^{-2}	4.4329×10^{-2}	6.5755×10^{-2}
		Present LBM	0.5	6.8152×10^{-3}	8.1523×10^{-3}	1.1963×10^{-2}	
			1.0	1.9632×10^{-2}	2.0196×10^{-2}	3.0721×10^{-2}	
			1.5	3.5074×10^{-2}	5.2597×10^{-2}	4.8376×10^{-2}	
	15	Present RLBM	0.5	7.4175×10^{-3}	7.8539×10^{-3}	1.1749×10^{-2}	2.3511×10^{-2}
			1.0	2.0575×10^{-2}	2.2402×10^{-2}	3.0116×10^{-2}	6.4079×10^{-2}
			1.5	3.4330×10^{-2}	3.8004×10^{-2}	4.7029×10^{-2}	
		Present LBM	0.5	8.4228×10^{-3}	1.0431×10^{-2}	1.1853×10^{-2}	
			1.0	2.3629×10^{-2}	2.7466×10^{-2}	3.0499×10^{-2}	
			1.5	4.2403×10^{-2}	4.8820×10^{-2}	4.8005×10^{-2}	
0.05	10	Present RLBM	0.5	6.5523×10^{-4}	9.8464×10^{-4}	2.7444×10^{-3}	4.5346×10^{-3}
			1.0	1.2211×10^{-3}	1.9854×10^{-3}	6.5336×10^{-3}	8.9663×10^{-3}
			1.5	1.8660×10^{-3}	2.9241×10^{-3}	9.9516×10^{-3}	1.2648×10^{-2}
		Present LBM	0.5	1.4508×10^{-3}	1.0663×10^{-3}	2.9100×10^{-3}	
			1.0	1.7079×10^{-3}	2.9279×10^{-3}	7.5728×10^{-3}	
			1.5	1.6802×10^{-3}	4.9443×10^{-3}	1.1879×10^{-2}	
	15	Present RLBM	0.5	8.4940×10^{-4}	7.4292×10^{-4}	1.7846×10^{-3}	3.1030×10^{-3}
			1.0	2.1072×10^{-3}	1.2356×10^{-3}	4.2660×10^{-3}	6.7396×10^{-3}
			1.5	3.5255×10^{-3}	2.1970×10^{-3}	6.9221×10^{-3}	9.9502×10^{-3}
		Present LBM	0.5	1.2797×10^{-3}	1.3320×10^{-3}	2.9066×10^{-3}	
			1.0	3.8932×10^{-3}	3.0506×10^{-3}	7.5078×10^{-3}	
			1.5	6.7043×10^{-3}	5.3264×10^{-3}	1.1740×10^{-2}	

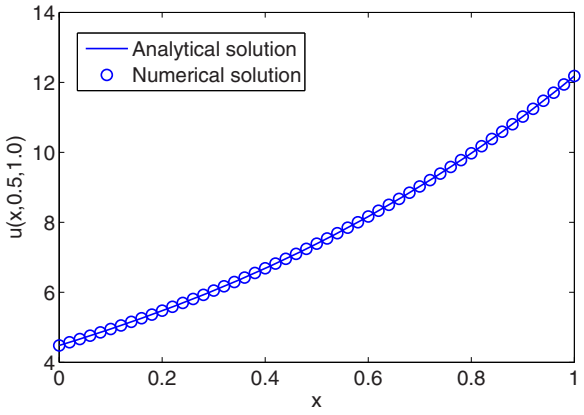

FIG. 10. (Color online) Numerical and analytical solutions of Example 3.6 at $t = 1.0$.

with the initial condition

$$p(x,y,0) = \frac{1}{\pi}\exp(-x^2 - y^2). \tag{50}$$

We carried out several simulations on the computational domain $[-5.0, 5.0] \times [-5.0, 5.0]$ with $\Delta x = 0.1$, $\Delta t = \pi/1000$. Here we use the same parameters reported in Ref. [34], and set $\varepsilon = 0.2$, $\varsigma = 0.1$, $L_{11} = 0$, and $L_{22} = 0.4$. Besides, the boundary condition is given by $p(x,y,t) = 0.0$ at any time t. We conducted some simulations, and present the results in Fig. 8. It can be seen that these numerical results are quantitatively in agreement with the results in Ref. [34], which demonstrate the capability of the present RLB model in solving the 2D Fokker-Planck equation.

Example 3.5. In this example, we consider a 2D NCDE with anisotropic diffusion and a source term [11]

$$\frac{\partial u}{\partial t} + \frac{\partial u^m}{\partial x} + \frac{\partial u^n}{\partial y} = D\left[d_1\frac{\partial^2 u}{\partial x^2} + d_2\frac{\partial^2 u}{\partial y^2} + 2d_3\frac{\partial u}{\partial x\partial y}\right] + F, \tag{51}$$

to test the present models. The problem has the following analytical solution with proper initial and boundary conditions:

$$u(x,y,t) = \operatorname{sech}[2(x + y - t)], \tag{52}$$

and the source term F is defined as

$$F = 2\vartheta(u - mu^m - nu^n) - 4Du(d_1 + d_2 + 2d_3)(2\vartheta^2 - 1), \tag{53}$$

where $\vartheta = \tanh[2(x + y - t)]$, d_1,d_2,d_3 and D are real constants. In our simulations, we will focus on the effect of the regularized procedure (see remark 2) on the stability and accuracy of the LB model.

The simulations are performed on $[-5,5] \times [-5,5]$ with $m = n = 2$, $d_1 = 1$, $d_2 = 2$, and $d_3 = 0$ or 1, which are the same as those used in Ref. [11]. We present the results in Fig. 9 where $D = 0.01$, $dx = 0.05$, $c = 10$, and $d_3 = 1$. It can be seen that the numerical result agrees well with the corresponding analytical solution. Besides, we would like to point out that both the present LBM and the model proposed in Ref. [10] are unstable, and do not work for this special case.

Furthermore, a more detailed comparison between present RLBM and present LBM is also conducted. The effects of the parameters D and d_3 are mainly considered since they have a great influence on the stability [11]. We present the results in Table V, and find that the GREs of different models increase in time, and the GREs decrease as the grid resolution increases. From Table V, one can also find that the present RLBM can produce a more accurate and more stable solution than the present LBM. Actually, for the case of $D = 0.01$ and $d_3 = 1.0$, the present LBMs are usually unstable, while the present RLBM almost still works which indicates that the use of the regularized procedure can produce more stable results.

In addition, we also noted that as pointed out in Ref. [11], the model in Ref. [10] is unstable for the case of $D = 0.01$ and $d_3 = 1.0$. To further show the superiority of the regularized model in stability, the regularized procedure is also used for the model in Ref. [10], and the numerical results are shown in Table VI. As seen from the Table VI, the model incorporated the regularized procedure works well except for the case of $D = 0.1$, $c = 15$, $t = 1.5$, while the model in Ref. [10] is unstable for all cases. From the above discussion, it is clear that the regularized procedure can be used to improve the stability of LB models.

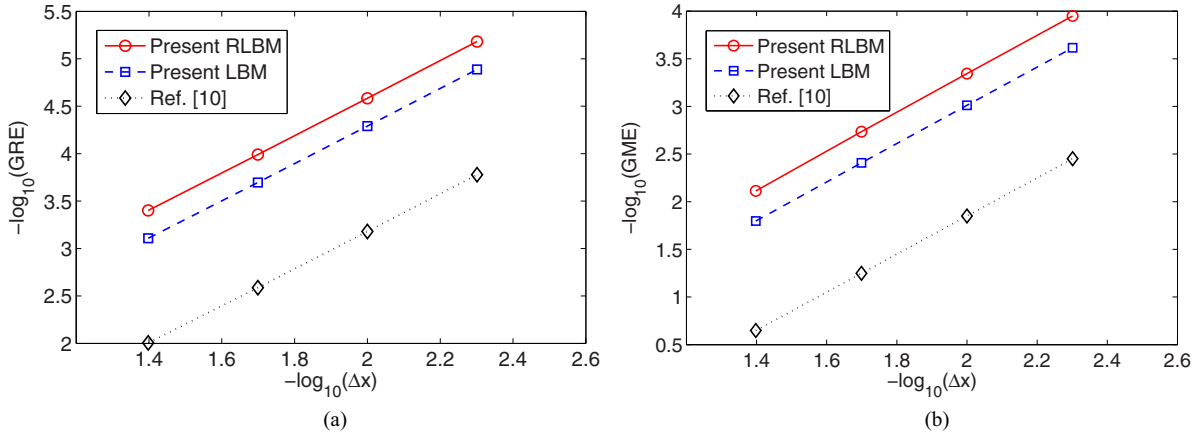

FIG. 11. (Color online) The errors of different models with different lattice steps for Example 3.6: (a) GREs, (b) GMEs.

TABLE VII. Comparison of the GREs at different time for Example 3.6.

Method	$t = 0.5$	$t = 1.0$	$t = 2.0$	$t = 4.0$	$t = 8.0$
Present RLBM	1.0233×10^{-4}	1.0233×10^{-4}	1.0233×10^{-4}	1.0233×10^{-4}	1.0233×10^{-4}
Present LBM	2.0134×10^{-4}	2.0140×10^{-4}	2.0140×10^{-4}	2.0140×10^{-4}	2.0140×10^{-4}
Ref. [10]	2.5839×10^{-3}	2.5851×10^{-3}	2.5851×10^{-3}	2.5851×10^{-3}	2.5851×10^{-3}

Example 3.6. We now consider the following NCDE with a source term:

$$\frac{\partial u}{\partial t} + \frac{\partial (10xu)}{\partial x} + \frac{\partial (10yu)}{\partial y} = \frac{\partial^2 u}{\partial x^2} + \frac{\partial^2 u}{\partial y^2} + [10(x+y)+19]u, \tag{54}$$

and the exact solution of the problem can be given as

$$u(x,y,t) = \exp(x+y+t). \tag{55}$$

In our simulations, the computational domain is fixed on $\Omega = [0,1] \times [0,1]$. We first presented the result at $t = 1$ and $y = 0.5$ in Fig. 10 where $\beta = 3.0$, $\Delta x = 0.02$, and $\Delta t = 2.0 \times 10^{-4}$. As seen from this figure, the numerical result is

in good agreement with the exact solution, and the corresponding GRE is 7.8752×10^{-6}. Besides, to test the convergence rate of different models, some simulations are also carried out at different lattice resolutions ($\Delta x = 1/25$ to $1/200$), and c is correspondingly changed from 40 to 320. We presented the GREs and GMEs at different resolutions in Fig. 11, where $t = 1.0$. As shown in this figure, the slopes of the fitting lines for the results are about 2, indicating that all of these three models have a second-order convergence rate in space. Besides, we also presented the GREs at different times in Table VII where $c = 80$, $\Delta x = 0.02$, and $\beta = 3.0$. From Table VII, it can be seen that the present RLBM is better than the other two models in accuracy. In addition, the effects of β and c are also studied. To this end, we calculated the GREs under different β and c, and presented the results in Table VIII. From this table, one can find that the errors of the present RLBM are less than those obtained by the other two models. And also, it is found that for $\beta = 3.0$ and $c = 160$, both the present LBM and the model in Ref. [10] are unstable, while the present RLBM works well, which indicates that the RLB model is more stable than the other three models. Finally, we investigated the relaxation time effect on the accuracy of different models, and present the results in Fig. 12 where $\Delta x = 0.02$, $\beta = 2.0$, $t = 1.0$. From this figure, it can be seen that the present RLBM performs better than the present LBM and the model in Ref. [10].

TABLE VIII. GREs of Example 3.6 with different β and c ($\Delta x = 0.02$, $t = 1.0$). (Blanks mean that the model is unstable.)

β	c	Present RLBM	Present LBM	Ref. [10]
0.9	80	1.3008×10^{-3}	5.7739×10^{-3}	4.2107×10^{-3}
	160	4.0288×10^{-4}	1.1375×10^{-3}	1.2299×10^{-3}
1.0	80	1.1086×10^{-3}	4.5622×10^{-3}	4.2952×10^{-3}
	160	3.2422×10^{-4}	8.5470×10^{-4}	1.2647×10^{-3}
2.0	80	3.3685×10^{-4}	8.6143×10^{-4}	3.3602×10^{-3}
	160	1.7524×10^{-5}	3.5957×10^{-5}	1.0789×10^{-3}
3.0	80	1.0233×10^{-4}	2.0140×10^{-4}	2.5851×10^{-3}
	160	1.2834×10^{-4}		

IV. CONCLUSIONS

In this paper, a regularized lattice Boltzmann model is developed for NCDEs with variable coefficients. Through the Chapman-Enskog analysis, it is shown that the NCDE can be recovered correctly from the present scheme without adopting any assumptions or auxiliary moments, which is different from some available LB models. We then tested the RLB model by using some classic NCDEs, and found that the numerical results agree well with the analytical or numerical solutions reported in some previous studies. Besides, it is also found that the present RLB model is more accurate and more stable than some available LB models, and has a second-order convergence rate in space. Finally, we would like to point out that the idea of the regularized procedure can be directly extended to the traditional LB models.

ACKNOWLEDGMENTS

The authors are grateful to referees for their valuable comments and suggestions. This work was supported by the National Natural Science Foundation of China (Grants No. 11272132 and No. 51576079) and the Natural Science Foundation of Hubei province (Grant No. 2015CFB440).

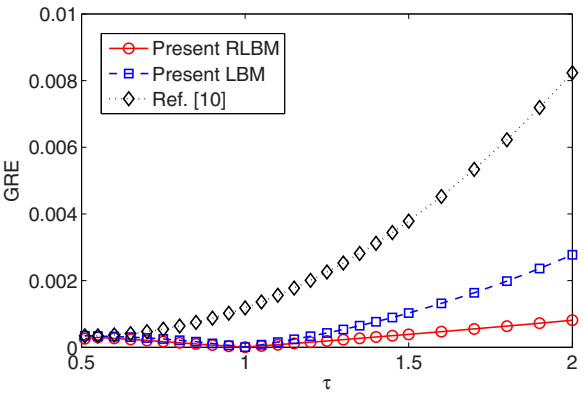

FIG. 12. (Color online) The GREs of different models at different relaxation time (Example 3.6).

[1] R. Benzi, S. Succi, and M. Vergassola, Phys. Rep. **222**, 145 (1992).
[2] S. Y. Chen and G. D. Doolen, Annu. Rev. Fluid Mech. **30**, 329 (1998).
[3] Z. L. Guo and C. Shu, *Lattice Boltzmann Method and its Application in Engineering* (World Scientific, Singapore, 2013).
[4] Z. H. Chai and B. C. Shi, Appl. Math. Modell. **32**, 2050 (2008).
[5] X. M. Yu and B. C. Shi, Appl. Math. Comput. **181**, 958 (2006).
[6] F. F. Wu, W. P. Shi, and F. Liu, Commun. Nonlin. Sci. Numer. Simul. **17**, 2776 (2012).
[7] P. J. Dellar, D. Lapitski, S. Palpacelli, and S. Succi, Phys. Rev. E **83**, 046706 (2011).
[8] R. G. M. van der Sman and M. H. Ernst, J. Comput. Phys. **160**, 766 (2000).
[9] B. C. Shi, B. Deng, R. Du, and X. W. Chen, Comput. Math. Appl. **55**, 1568 (2008).
[10] B. C. Shi and Z. L. Guo, Phys. Rev. E **79**, 016701 (2009).
[11] B. C. Shi and Z. L. Guo, Comput. Math. Appl. **61**, 3443 (2011).
[12] I. Ginzburg, Adv. Water Resour. **28**, 1171 (2005).
[13] I. Ginzburg, Adv. Water Resour. **51**, 381 (2013).
[14] I. Rasin, S. Succi, and W. Miller, J. Comput. Phys. **206**, 453 (2005).
[15] H. Yoshida and M. Nagaoka, J. Comput. Phys. **229**, 7774 (2010).
[16] B. Chopard, J. L. Falcone, and J. Latt, Eur. Phys. J.: Spec. Top. **171**, 245 (2009).
[17] Z. H. Chai and T. S. Zhao, Phys. Rev. E **87**, 063309 (2013).
[18] P. Asinari and I. V. Karlin, Phys. Rev. E **81**, 016702 (2010).
[19] C. Aidun and J. Clausen, Annu. Rev. Fluid Mech. **42**, 439 (2010).
[20] H. Liang, Z. H. Chai, B. C. Shi, Z. L. Guo, and T. Zhang, Phys. Rev. E **90**, 063311 (2014).
[21] D. Y. Gao, Z. Q. Chen, and L. H. Chen, Int. J. Heat Mass Transfer **70**, 979 (2014).
[22] Z. H. Chai and T. S. Zhao, Phys. Rev. E **90**, 013305 (2014).
[23] J. Wang, D. Wang, P. Lallemand, and L.-S. Luo, Comput. Math. Appl. **65**, 262 (2013).
[24] P. Lallemand and L.-S. Luo, Phys. Rev. E **61**, 6546 (2000).
[25] B. Servan-Camas and F. T.-C. Tsai, J. Comput. Phys. **228**, 236 (2009)
[26] J. Latt and B. Chopard, Math. Comput. Simul. **72**, 165 (2006).
[27] F. Higuera, S. Succi, and R. Benzi, Eur. Phys. Lett. **9**, 345 (1989).
[28] A. Montessori, G. Falcucci, P. Prestininzi, M. La Rocca, and S. Succi, Phys. Rev. E **89**, 053317 (2014).
[29] L. Axner, J. Latt, A. G. Hoekstra, B. Chopard, and P. M. A. Sloot, Int. J. Mod. Phys. C **18**, 661 (2007).
[30] X. Q. Xiang, Z. H. Wang, and B. C. Shi, Commun. Nonlin. Sci. Numer. Simul. **17**, 2415 (2012).
[31] Z. L. Guo, C. G. Zheng, and B. C. Shi, Chin. Phys. **11**, 366 (2002).
[32] G. W. Wei, J. Phys. A: Math. Gen. **33**, 4935 (2000).
[33] A. Kurganov and E. Tadmor, J. Comput. Phys. **160**, 241 (2000).
[34] M. Dehghan and V. Mohammadi, Eng. Anal. Bound. Elem. **47**, 38 (2014).